

Seismic shear behavior of rectangular hollow bridge columns

Y.L. Mo[†] and Chyuan-Hwan Jeng[‡]

Department of Civil and Environmental Engineering, University of Houston, Houston, Texas, U.S.A.

S.F. Perng^{‡†}

Department of Civil Engineering, National Kaohsiung Institute of Technology, Kaohsiung, Taiwan

Abstract. An analytical model incorporating bending and shear behavior is presented to predict the lateral loading characteristic for rectangular hollow columns. The moment-curvature relationship for the rectangular hollow sections of a column is firstly determined. Then the nonlinear lateral load-displacement relationship for the hollow column can be obtained accordingly. In this model, thirteen constitutive laws for confined concrete and five approaches to estimate the shear capacity are used. A series of tests on 12 model hollow columns aimed at the seismic shear behavior are reported, and the test data are compared to the analytical results. It is found that the analytical model reflects the experimental results rather closely.

Key words: hollow bridge column; shear behavior; seismic behavior; confined concrete; ductility factor; load-displacement relationship.

1. Introduction

Unlike those of buildings, columns of bridges are usually designed as the first structural elements to undergo excessive plastic deformation ultimately under severe earthquake attacks. That is, columns are expected to be the primary elements of bridges to dissipate seismic energy through their high ductility demanded implicitly by design codes. Failure of bridge columns would often cause collapse or falling of bridge spans, as was the very scenario for the majority of the damages of bridges during the tragic Chi-Chi Earthquake of Taiwan on September 21, 1999. Thus the behavior of columns does play essential role for bridge structures to resist earthquake attacks.

To maximize structural efficiency in terms of the strength/mass and stiffness/mass ratios and to reduce the mass contribution of the column to seismic response (Priestly *et al.* 1996), it has been a popular engineering practice to use a hollow section for bridge columns, especially for tall columns. In contrast to the popularity in practice, researches on the structural behavior of hollow columns are limited. In the past two decades, Mander (1983) conducted an experimental investigation on four hollow column specimens at the University of Canterbury in New Zealand; Taylor (Taylor *et al.*

[†] Professor

[‡] Ph.D. Student

^{‡†} Associate Professor

1994) studied the static behavior of thin-walled box piers; Matsuda (Matsuda *et al.* 1996) performed seismic model tests on hollow piers.

Besides the scarcity of researches, the effect of the particular configuration of transverse steel in the hollow section used in the bridge columns in Taiwan was never investigated. Since 1997, Mo (1998) has been proceeding with a series of both experimental and theoretical investigations into the structural behavior of reinforced concrete hollow columns with an emphasis on the effect of the transverse steel configuration of hollow columns of Taiwan. The stress-strain characteristic of confined concrete of hollow columns was experimentally investigated (Hong 1998). The flexural response was investigated and models for prediction have been proposed (Yao 1998, Wang 1999). The shear behavior was studied (Mo and Jeng 1999).

In this paper, an analytical model incorporating both bending and shear behavior is presented to predict the lateral loading characteristic for rectangular hollow columns. The moment-curvature relationship for the rectangular hollow sections of a column is firstly determined. Then the nonlinear lateral load-displacement relationship (the so-called primary curve) for the hollow column can be obtained accordingly. Also, observed experimental results from a series of tests on 12 model columns aimed at the shear behavior are compared to those from the proposed analytical model. The analytical model is found to be able to reflect the experimental results rather closely.

2. Analytical model

2.1 Constitutive laws of materials

2.1.1 Concrete

A number of constitutive laws of confined concrete have been proposed over the past three decades. In this investigation, nine constitutive models for normal strength concrete (Table 1) and four constitutive models for high strength concrete (Table 2) are employed. Their predicted results are evaluated by tests. The parameters used in each model are mentioned below.

Unconfined Kent and Park (1971) model did not consider confinement of concrete. Confined Kent and Park (1971) model supposed the confined concrete raised its maximum strength and maintained its residual strength $0.2 f_c'$ at large strain. Modified Kent and Park model (Park *et al.* 1982) modified their last model to let the confined concrete increase its initial stiffness. Muguruma *et al.* (1978a, 1978b) model was similar to the Confined Kent and Park model with different stress-strain curve shape except having a ultimate confined concrete strain. Sheikh and Uzumeri (1980, 1982) model was similar to the Modified Kent and Park model except having a flat ultimate strength within a strain range. The parameters of the Sheikh and Uzumeri model were affected by the effectively confined core area which were based on tests of square specimens. Mander *et al.* (1988a, 1988b) model used confining pressure to affect the shape of the stress-strain curve. The confining pressure was affected by the effectively confined core area which were based on tests of rectangular specimens. Fujii *et al.* (1988) model was similar to the Muguruma *et al.* model, but had different control parameters. Saatcioglu and Razvi (1992) model seemed to modify the Modified Kent and Park model with effective confining pressures of both directions of the rectangular cross section. Hoshikuma *et al.* (1997) model did not use the concept of the effectively confined core area and had residual strength $0.5 f_c'$ at large strain. Sheikh, Shah and Khoury's (1994) model was established by testing 120 standard cylindrical specimens made of high strength concrete, and did

Table 1 Constitutive models for normal strength concrete

Model	Stress-strain model for confined concrete			Applicable cross-sectional shape
	Ascending branch	Falling branch	Residual stress	
Unconfined Kent and Park (1971)	$f_c = f_c' \left[\frac{2\varepsilon}{0.002} - \left(\frac{\varepsilon}{0.002} \right)^2 \right]$	$f_c = f_c' [1 - Z(\varepsilon - 0.002)]$	–	Square
Confined Kent and Park (1971)	$f_c = f_c' \left[\frac{2\varepsilon}{0.002} - \left(\frac{\varepsilon}{0.002} \right)^2 \right]$	$f_c = f_c' [1 - Z(\varepsilon - 0.002)]$	20% of f_c'	Square
Modified Kent and Park (1982)	$f_c = Kf_c' \left[\frac{2\varepsilon}{0.002K} - \left(\frac{\varepsilon}{0.002K} \right)^2 \right]$	$f_c = Kf_c' [1 - Z_m(\varepsilon - 0.002K)]$	20% of Kf_c'	Square
Muguruma <i>et al.</i> (1980)	$f_c = E_c \varepsilon + \frac{f_c' - E_c \varepsilon_c}{\varepsilon_c^2} \varepsilon^2$ $f_c = \frac{f_c' - f_{cc}}{(\varepsilon_c - \varepsilon_{cc})} (\varepsilon - \varepsilon_{cc})^2 + f_{cc}$	$f_c = \frac{f_{cu} - f_{cc}}{(\varepsilon_{cu} - \varepsilon_{cc})} (\varepsilon - \varepsilon_{cc}) + f_{cc}$	–	Circle Square
Sheikh and Uzumeri (1982)	$f_c = f_{cc} \left[\frac{2\varepsilon}{\varepsilon_{s1}} - \left(\frac{\varepsilon}{\varepsilon_{s1}} \right)^2 \right]$	$f_c = f_{cc} [1 - Z(\varepsilon - \varepsilon_{s2})]$	30% of f_{cc}	Square
Mander <i>et al.</i> (1988a,b)	$f_c = \frac{f_{cc} x^r}{r - 1 + x^r}$	$f_c = \frac{f_{cc} x^r}{r - 1 + x^r}$	–	Circle Square Wall-type
Fujii <i>et al.</i> (1988)	$f_c = E_c \varepsilon + \frac{f_{cc} - E_c \varepsilon_c}{\varepsilon_c^2} \varepsilon^2$ $f_c = \frac{f_c' - f_{cc}}{(\varepsilon_c - \varepsilon_{cc})^3} (\varepsilon - \varepsilon_{cc})^3 + f_{cc}$	$f_c = f_{cc} - \theta(\varepsilon - \varepsilon_{cc})$	20% of f_{cc}	Circle Square
Saatcioglu and Razvi (1992)	$f_c = f_{cc} \left[2 \left(\frac{\varepsilon}{\varepsilon_{cc}} \right) - \left(\frac{\varepsilon}{\varepsilon_{cc}} \right)^2 \right]^{1/(1+2K)}$	$f_c = f_{cc} - \frac{0.15 f_{cc}}{\varepsilon_{85} - \varepsilon_{cc}} (\varepsilon - \varepsilon_{cc})$	20% of f_{cc}	Circle Square Wall-type
Hoshikuma <i>et al.</i> (1997)	$f_c = E_c \varepsilon \left[1 - \frac{1}{n} \left(\frac{\varepsilon}{\varepsilon_{cc}} \right)^{n-1} \right]$	$f_c = f_{cc} - E_{des} (\varepsilon - \varepsilon_{cc})$	50% of f_{cc}	Circle Square

not incorporate confinement effect. Diniz *et al.* (1997) modified the model proposed by Fafits and Shah in 1985 for high strength concrete. Cusson and Paultre (1995) refined the concept of confinement index (Park *et al.* 1982, Muguruma *et al.* 1983, Saatcioglu *et al.* 1993) and proposed the so-called effective confinement index, and established their stress-strain model accordingly. Modified Razvi and Saatcioglu (1999) model basically modified the descending branch of Saatcioglu and Rzvi (1992) model.

2.1.2 Reinforcing steel

A typical monotonic (tensile) stress-strain curve of reinforcing steel consists of three segments, namely, elastic linear branch, yielding plateau, and strain hardening branch. When reversed (tension-compression) axial loading is applied, however, the well-known Bauschinger effect emerges and the

Table 2 Constitutive models for high strength concrete specimens

Model	Stress-strain model for confined concrete			Applicable cross-sectional shape
	Ascending branch	Falling branch	Residual stress	
Sheikh, Shah and Khoury (1994)	$f_c = f_c' \sum_{i=1}^{i=3} a_i \left(\frac{\epsilon_c}{\epsilon_0} \right)^i$ $a_1=1.25, a_2=0.31, a_3=-0.56$	$f_c = f_c' \sum_{i=1}^{i=3} a_i \left(\frac{\epsilon_c}{\epsilon_0} \right)^i$ $a_1=-72.7, a_2=147.5, a_3=-73.8$	–	Rectangle
Modified Fafits and Shah (1997)	$f_c = f_{cc}' \left[1 - \left(1 - \frac{\epsilon_c}{\epsilon_{cc}} \right)^A \right]$	$f_c = f_{cc}' \exp \left[-K(\epsilon_c - \epsilon_{cc})^{1.15} \right]$	–	Square
Cusson and Pultre (1995)	$f_c = f_{cc} \frac{k(\epsilon_c/\epsilon_{cc})}{k-1+(\epsilon_c/\epsilon_{cc})^k}$	$f_c = f_{cc} \cdot \exp \left[k_1(\epsilon_c - \epsilon_{cc})^{k_2} \right]$	–	Square
Modified Razvi and Saatcioglu (1999)	$f_c = \frac{f_{cc}' \left(\frac{\epsilon_c}{\epsilon_1} \right)^r}{r-1 + \left(\frac{\epsilon_c}{\epsilon_1} \right)^r}$	$f_c = f_{cc}' \frac{0.15 f_{cc}'}{\epsilon_{85} - \epsilon_1} (\epsilon_c - \epsilon_1)$	20% of f_{cc}	Circle Square Wall-type

stress-strain curve becomes nonlinear at a stress lower than the initial yield strength (Park and Paulay 1975). In this study, the softened branch relation proposed by Mander (1983) to describe the Bauschinger effect on the reversed stress-strain behavior is used.

In addition, the buckling effect of rebars (also called low-cycle fatigue) is a phenomenon that has been identified experimentally and theoretically (Monti and Nuti 1992, Mander *et al.* 1994, and Rodriguez *et al.* 1999). As the slenderness ratio of rebars becomes larger, which is usually the case for reduced-scale model tests, this effect gets more prominent and can not be ignored. Therefore it is also taken into account in the analytical model by using a reduction factor according to the tests of Mander *et al.* (1994).

2.2 Moment-curvature analysis

Based on the equilibrium of internal forces of the cross section and the assumption of the linear distribution of normal strain (plane section remains plane after bending), the section characteristic is determined by conventional moment-curvature analysis for a cross section of RC members iteratively. Through this analysis, such sectional parameters for the cracking state (M_{cr} , ϕ_{cr}), yielding state (M_y , ϕ_y), and ultimate state (M_u , ϕ_u) are obtained, and a trilinear idealization (Mo 1994) can be made for the moment-curvature curve for the section.

2.3 Loading-displacement relationship

The entire load-displacement relationship can be divided into two parts, namely, ascending and descending branches, and can be determined by the moment-area method as shown in Appendix I.

2.4 Shear capacity

Five approaches to estimate the shear capacity are used, including ACI 318-95 Code Provisions,

UCB equations (Aschheim *et al.* 1992), UCSD equations (Priestley *et al.* 1994), Caltrans model (Caltrans 1995), and USC formulae (Xiao *et al.* 1998). Note that the USC approach is a modification of the UCSD equations, in which the k coefficient is modified to suit for high strength concrete. In this paper, the USC approach is used for high strength concrete specimens only. The predicted results by the five approaches are compared with the experimental results.

Except for the ACI 318-95 approach, it is recognized that the shear capacity varies with the displacement ductility factor. So the shear capacity is calculated point by point along the loading-displacement curve.

3. Experimental program

Twelve reinforced concrete hollow columns were tested under a constant axial force varying from 0.054 to 0.255 $f_c' A_g$ and a cyclically reversed horizontal load. Primary test parameters include failure mode (transverse reinforcement and/or shear span), concrete compressive strength, and axial force level.

3.1 Specimens

The column and foundation of each of the specimens were designed according to the seismic provisions (ACI 1995). Properties of the specimens are shown in Table 3. Fig. 1 indicates the dimensions and reinforcement configuration of the specimens. Note that this configuration of transverse reinforcement has been used currently in bridge design in Taiwan. The cross section of each specimen is 500 × 500 mm; the length and wall thickness of the hollow column, are 2.2 m and 120 mm, respectively. The first character of the specimen name stands for the concrete compressive strength (Normal or Higher). In this paper the spacing of the confining reinforcement satisfies both

Table 3 Properties of the specimens

Specimen No.	f_c' (Mpa)	$\frac{P}{f_c' A_g}$	Shear span (mm)	Longitudinal reinforcement		Shear reinforcement (in plastic hinge region)				Confining reinforcement (in plastic hinge region)			
				bar no.	f_y (MPa)	dia. (mm)	f_y (MPa)	Spacing (mm)	$\frac{A_v}{A_{v, req'd}}$	dia. (mm)	f_y (MPa)	Spacing (mm)	$\frac{A_{sh}}{A_{sh, req'd}}$
NS1	32.6	0.093	1800	#3	476	6	480	50	1.62	6	480	50	1.50
NS2	30.6	0.176	1800	#3	476	6	480	50	1.75	6	480	50	1.50
NI1-a	33.6	0.086	1800	#3	476	3	405	50	0.40	5	350	50	0.51
NI2-a	29.4	0.185	1800	#3	476	3	405	50	0.44	5	350	50	0.51
NI1-b	20.2	0.136	1500	#3	476	3	405	50	0.35	5	350	50	0.51
NI2-b	21.4	0.256	1500	#3	476	3	405	50	0.37	5	350	50	0.51
HS1	58.1	0.092	1800	#3	476	6	480	50	2.79	6	480	50	1.15
HS2	62.5	0.129	1800	#3	476	6	480	50	3.02	6	480	50	1.15
HI1-a	70.0	0.077	1800	#3	476	4	363	40	0.60	6	480	40	0.48
HI2-a	61.1	0.132	1800	#3	476	4	363	40	0.66	6	480	40	0.48
HI1-b	50.5	0.106	1500	#3	476	4	363	40	0.52	6	480	40	0.48
HI0-b	49.7	0.054	1500	#3	476	4	363	40	0.50	6	480	40	0.48

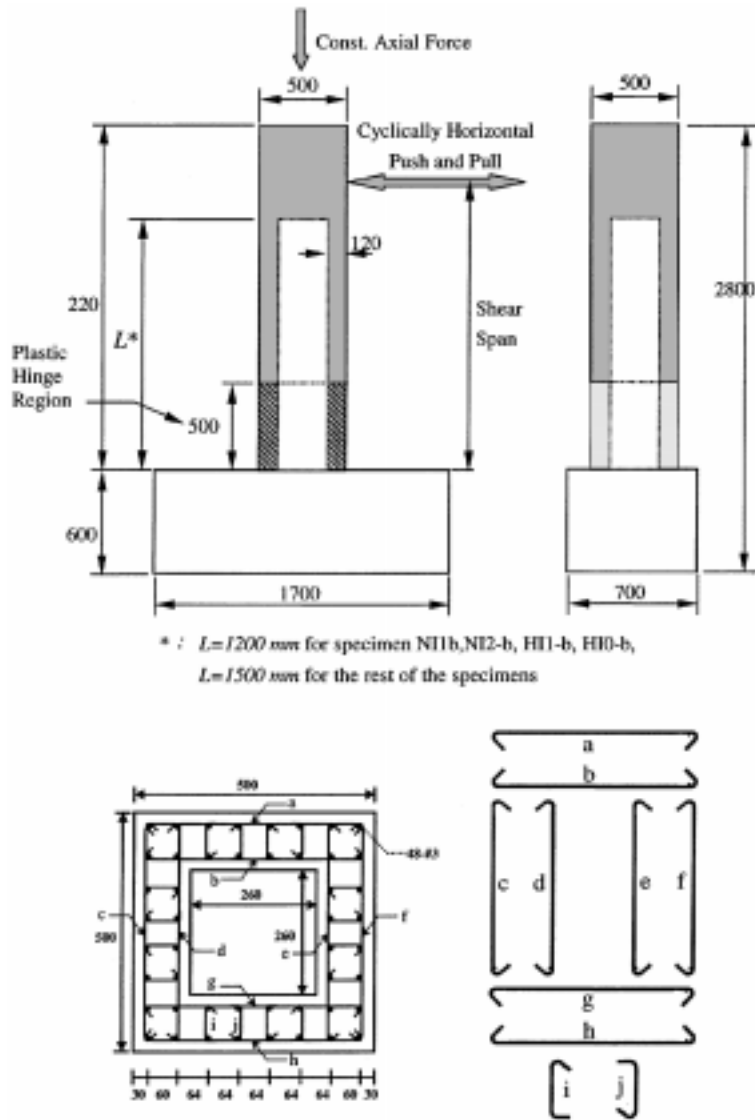


Fig. 1 Illustration of the outline, dimensions, and reinforcement configuration of the specimens (Unit: mm)

the design requirements of ACI code (ACI 1995), and the requirements to prevent buckling suggested by Priestley *et al.* (1996), in which the spacing needs to be less than six times the diameter of longitudinal rebars. However, the provided shear reinforcement of the specimens with an expected shear failure is much less than that required by the ACI code (ACI 1995). The four specimens with an expected flexural failure mode serve mainly as control of comparison.

3.2 Test setup and loading sequence

A schematic drawing of the test setup is shown in Fig. 2. The specimen was mounted vertically with the bottom of the reinforced concrete foundation being held by a steel foundation, and the end

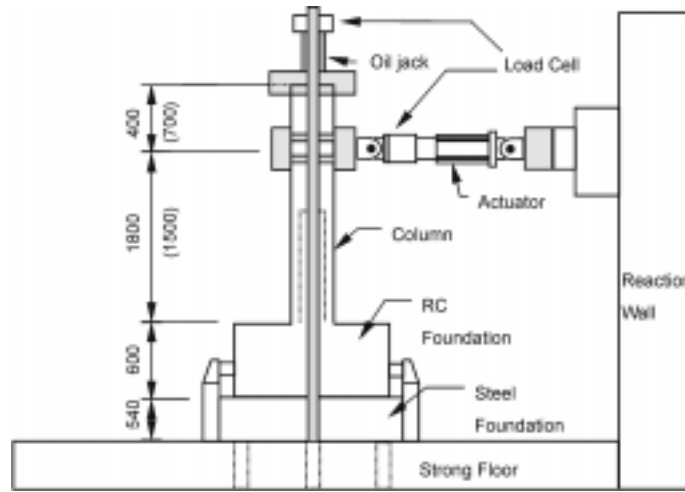


Fig. 2 Schematic drawing of the test setup (unit: mm)

of the column was held by a hydraulic jack to provide a constant axial force. Under the hydraulic jack the column was held by an actuator, which was horizontally mounted to a reaction wall. The actuator had a capacity of 500 kN and was capable of moving the column 150 mm in both positive and negative directions. A displacement of 150 mm corresponds to a columns drift (ratio of horizontal displacement to column length) of 8.3 percent. Each specimen was instrumented with load cells, displacement transducers, and strain gages to monitor the applied displacements and corresponding loads as well as the resulting strains and relative deformations.

The specimens were tested under displacement control, following a predetermined displacement history defined in terms of column drift percentage. The displacement routine, shown in Fig. 3, consists of cycles with column drifts up to 6.1 percent. The displacement cycles were repeated to measure the strength degradation.

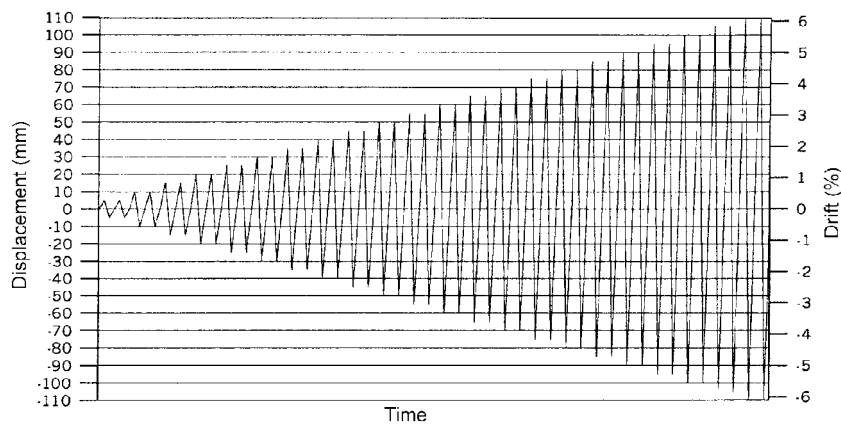


Fig. 3 Loading history

4. Experimental results

4.1 General observations

All twelve hollow columns developed stable responses up to certain displacement ductility levels. Flexural cracks perpendicular to the column axis developed first in regions close to the bottom end of the columns. The flexural cracks became inclined and extended into the web zone of the columns due to the influence of shear, typically at a stage exceeding the first yield of longitudinal rebars. At later stages of loading, typically at displacement ductility levels of 2 and 3, independent shear

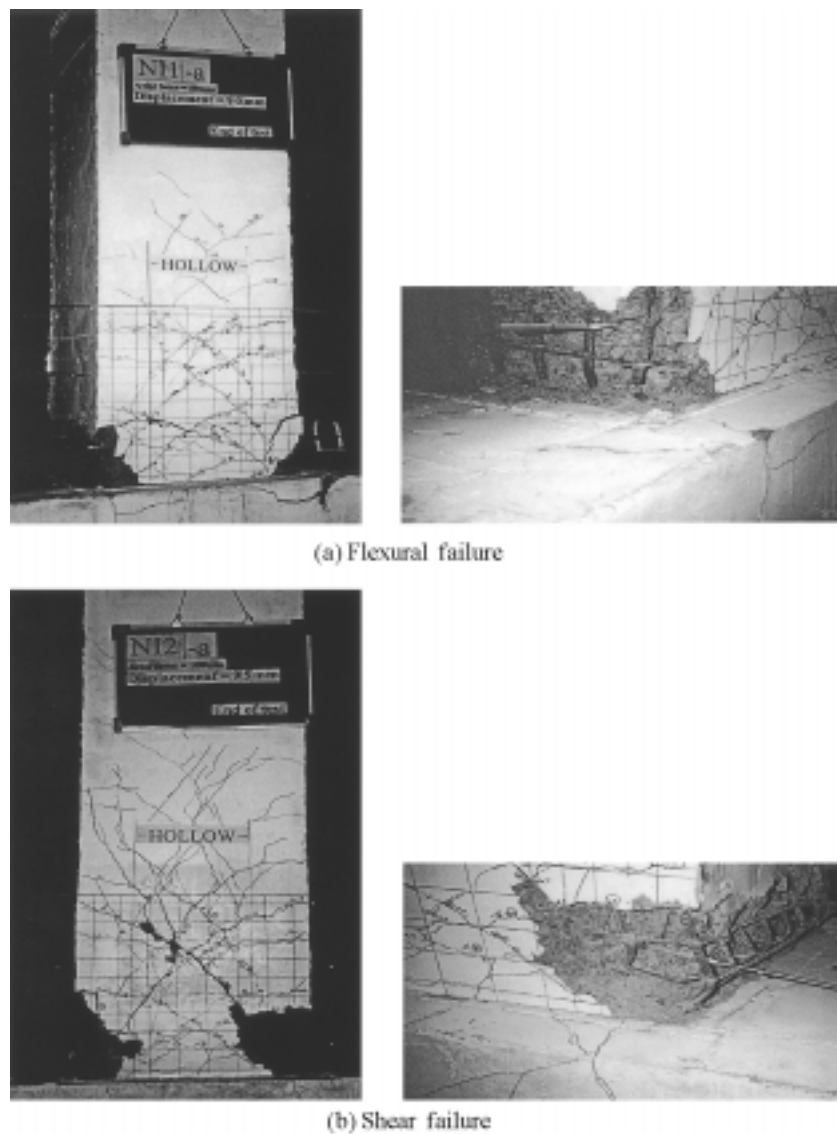


Fig. 4 Failure modes

cracks started to occur. Plastic hinges were fully formed at the bottom end of the columns, which contributed to the development of ductility. Although all of the specimens developed the estimated flexural strength, their ultimate performances and the ductility levels achieved were different for different testing conditions. As shown in Fig. 4, for example, the ultimate failure modes for Specimens NI1-a and NI2-a were developed according to either of the following two scenarios.

4.2 Flexural failure

Specimen NI1-a was reinforced with forty-eight No.3 ($\phi = 9.5$ mm) longitudinal rebars and lateral ties of 5 mm diameter at a 50 mm center-to-center spacing, and was subjected to an axial force of $0.086 f_c' A_g$. Because the axial force is small, the specimen developed displacement ductility factor of 4.6. The longitudinal rebars had buckled slightly before they ruptured. The ultimate performance for this specimen was dominated by flexure due to the rupture of longitudinal rebars at the bottom end of the columns, as shown in Fig. 4(a). According to the specimen design, this specimen was expected to fail in shear. However, it failed in flexure. This means that the actual shear capacity of this specimen is much higher than that specified in the ACI code.

4.3 Shear failure

Specimen NI2-a had the same longitudinal rebars and lateral ties as Specimen NI1-a. However, the axial force on the specimen ($0.185 f_c' A_g$) was greater than that on Specimen NI1-a. Therefore, the developed displacement ductility factor of this specimen (4.4) was less than that of Specimen NI1-a. Right before shear failure, this specimen had similar performance to Specimen NI1-a. At the ultimate state, this specimen failed due to a very clear shear crack through the plastic hinge region, as shown in Fig. 4(b).

4.4 Effect of concrete compressive strength

Table 4 indicates that specimens with higher concrete compressive strength have greater maximum lateral force as expected. However, it can be seen from Table 4 that higher concrete compressive strength decreases displacement ductility factor. The reason for this is that higher concrete compressive strength increases the yielding displacement.

The ductility factor is defined as the displacement at the eighty percent of the maximum horizontal force in the descending portion divided by the displacement at the occurrence of longitudinal steel yielding. Table 4 also gives the experimental results of the ductility factor for all of the specimens. It can be seen from Table 4 that the range of ductility factor for twelve specimens is from 3.7 to 5.3.

4.5 Effect of axial force

When Specimen NI1-a is compared to Specimen NI2-a, it can be found from Table 4 that greater axial force produces greater maximum lateral force and less ductility factor. The same conclusion can be found when both Specimens HI1-a and HI2-a are compared. Also the failure mode will be changed from flexural failure to shear failure when greater axial force is applied.

Table 4 Experimental results

Specimen No.	Yielding displacement (mm)	Yielding force (kN)	Ultimate displacement (mm)	Maximum force (kN)	Ductility factor	Energy dissipation (kN-mm)	Failure mode
NS1	16.8	208.8	88.7	270.9	5.3	391640.8	Flexural
NS2	17.2	244.1	85.3	315.2	4.9	346829.8	Flexural
NI1-a	18.2	203.3	83.9	261.6	4.6	276522.8	Flexural
NI2-a	17.9	207.4	77.4	289.5	4.4	224869.7	Shear
NI1-b	15.1	230.6	63.5	270.1	4.2	190572.3	Shear
NI2-b	13.5	248.6	50.3	297.4	3.7	101967.5	Shear
HS1	18.2	250.0	83.6	333.3	4.6	327429.7	Flexural
HS2	18.4	295.7	78.9	360.3	4.3	310707.8	Flexural
HI1-a	19.1	280.3	86.8	332.2	4.5	318895.4	Flexural-Shear
HI2-a	19.1	293.8	73.6	350.2	3.9	219028.2	Shear
HI1-b	15.7	321.6	69.3	363.6	4.4	258143.8	Shear
HI0-b	15.1	254.9	71.2	302.3	4.7	345544.1	Flexural

5. Comparison of analytical results with experimental data

The analytical model is verified by the series of tests on 12 model columns.

5.1 Effect of constitutive models

As mentioned previously, the provided spacing in each specimen precluded buckling of the longitudinal rebars. Therefore, the predicted results by using the thirteen constitutive models of confined concrete are compared with experimental results. The comparisons of the maximum lateral force P_u , the ultimate lateral displacement δ_u , and the displacement ductility factor are shown in Table 5 for the specimens with normal strength concrete and Table 6 for the specimens with high strength concrete. The typical lateral load-displacement curves are shown in Fig. 6 and Fig. 7. Note that the experimental curves in Figs. 6 and 7 are the envelopes of the hysteretic loops of Specimens NI1-a and HI1-a, as shown in Fig. 5. It is found from Tables 5 and 6 that modified Kent and Park model has the closest results with tests for both normal and high strength concrete specimens. However, the Sheikh and Uzumeri's model gives also a good correlation with the test results for normal strength concrete, as shown in Table 5.

5.2 Estimation of shear capacity

Eight out of the twelve specimens have insufficient shear and confining reinforcements. The comparisons between the theoretical shear capacities and the experimental curves for these eight specimens are plotted in Figs. 8 and 9. In Figs. 8 and 9, the lateral deformation capacity is obtained from the corresponding deformation at the 80% of the maximum lateral force in the descending branch. For the specimens with shear failure the shear capacity is the force in each specimen when shear failure occurred. For example, the shear failure of each of specimens NI1-a, NI2-a and HI2-a is marked in Fig. 5. However, this shear capacity will reduce with increasing ductility. It should be

Table 5 Comparison of test data with analytical results for normal strength concrete specimens

Analytical Model		Specimen No.						Average	Coeff. of Variance
		NS1	NS2	NI-1-a	NI-2-a	NI-1-b	NI-2-b		
Unconfined Kent and Park (1971)	P_{u_ana}/P_{u_exp}	0.85	0.79	0.88	0.84	0.86	0.85	0.845	0.091%
	$\Delta_{u_ana}/\Delta_{u_exp}$	0.25	0.24	0.27	0.25	0.25	0.22	0.247	0.027%
	$\mu_{\Delta_ana}/\mu_{\Delta_exp}$	0.21	0.22	0.24	0.24	0.27	0.32	0.250	0.160%
Confined Kent and Park (1971)	P_{u_ana}/P_{u_exp}	0.95	0.90	0.97	0.91	1.01	0.93	0.945	0.167%
	$\Delta_{u_ana}/\Delta_{u_exp}$	1.05	0.94	0.73	0.67	0.69	0.61	0.782	3.002%
	$\mu_{\Delta_ana}/\mu_{\Delta_exp}$	0.87	0.74	0.67	0.53	0.65	0.44	0.650	2.308%
Modified Kent and Park (1982)	P_{u_ana}/P_{u_exp}	0.99	0.98	0.99	0.98	1.08	1.04	1.010	0.168%
	$\Delta_{u_ana}/\Delta_{u_exp}$	1.21	1.05	1.01	0.81	0.71	0.72	0.918	4.106%
	$\mu_{\Delta_ana}/\mu_{\Delta_exp}$	1.03	0.88	0.92	0.66	0.72	0.59	0.800	2.876%
Muguruma <i>et al.</i> (1980)	P_{u_ana}/P_{u_exp}	0.98	0.96	0.98	0.95	1.07	1.02	0.993	0.199%
	$\Delta_{u_ana}/\Delta_{u_exp}$	1.18	0.94	0.63	0.61	0.71	0.65	0.787	5.171%
	$\mu_{\Delta_ana}/\mu_{\Delta_exp}$	0.99	0.75	0.57	0.48	0.70	0.51	0.667	3.627%
Sheikh and Uzuemi (1982)	P_{u_ana}/P_{u_exp}	0.98	0.97	0.99	1.00	1.10	1.09	1.022	0.334%
	$\Delta_{u_ana}/\Delta_{u_exp}$	1.27	1.22	1.21	1.12	0.88	1.00	1.117	2.251%
	$\mu_{\Delta_ana}/\mu_{\Delta_exp}$	1.04	0.97	1.08	0.89	0.88	0.82	0.947	1.015%
Mander <i>et al.</i> (1988)	P_{u_ana}/P_{u_exp}	1.00	0.99	0.98	0.94	1.06	0.99	0.993	0.151%
	$\Delta_{u_ana}/\Delta_{u_exp}$	1.27	1.18	0.58	0.51	0.95	0.49	0.830	12.220%
	$\mu_{\Delta_ana}/\mu_{\Delta_exp}$	1.06	0.97	0.53	0.41	0.93	0.39	0.715	9.263%
Fujii <i>et al.</i> (1988)	P_{u_ana}/P_{u_exp}	0.96	0.92	0.97	0.91	1.02	0.94	0.953	0.159%
	$\Delta_{u_ana}/\Delta_{u_exp}$	1.12	0.76	0.53	0.41	0.54	0.45	0.635	7.115%
	$\mu_{\Delta_ana}/\mu_{\Delta_exp}$	0.91	0.60	0.47	0.32	0.50	0.35	0.525	4.603%
Saatcioglu and Razvi (1992)	P_{u_ana}/P_{u_exp}	0.98	0.97	0.98	0.94	1.04	0.97	0.980	0.108%
	$\Delta_{u_ana}/\Delta_{u_exp}$	1.22	1.07	0.63	0.50	0.45	0.42	0.715	11.835%
	$\mu_{\Delta_ana}/\mu_{\Delta_exp}$	1.02	0.85	0.57	0.39	0.42	0.33	0.597	7.783%
Hoshikuma <i>et al.</i> (1997)	P_{u_ana}/P_{u_exp}	0.98	0.97	0.98	0.94	1.06	0.99	0.987	0.159%
	$\Delta_{u_ana}/\Delta_{u_exp}$	1.31	1.11	0.72	0.56	1.04	0.57	0.885	9.747%
	$\mu_{\Delta_ana}/\mu_{\Delta_exp}$	1.05	0.83	0.63	0.43	0.96	0.44	0.723	6.983%

P_{u_ana} : maximum force calculated by specified analytical model

P_{u_exp} : maximum force obtained from the experiment curve

Δ_{u_ana} : displacement corresponding to $0.8P_{max}$ or ultimate displacement calculated by specified analytical model

Δ_{u_exp} : displacement corresponding to $0.8P_{max}$ obtained from experiment

μ_{Δ_ana} : displacement ductility calculated by specified analytical model

μ_{Δ_exp} : displacement ductility obtained from experiment curve

noted that the shear capacity predicted by the ACI code is less than (conservative) the actual capacity, as shown in Specimen NI2-a of Fig. 8.

For the specimens with normal strength concrete, it can be seen from Fig. 8 that ACI 318-95 approach is too conservative, while Caltrans model overestimate the shear capacities. The UCSD approach proposed by Priestly *et al.* gives predictions very close to the experimental results.

For the specimens with high strength concrete, Fig. 9 reveals that nearly all the approaches would possibly overestimate the shear capacities, except for the USC approach proposed by Xiao *et al.*,

Table 6 Comparison of test data with analytical results for high strength concrete specimens

Specimen No.		HS1	HS2	HI-1-a	HI-2-a	HI-1-b	HI-0-b	Average	Coeff. of Variance
Analytical Model									
Unconfined Kent and Park (1971)	P_{u_ana}/P_{u_exp}	0.90	0.95	0.95	0.91	0.92	0.96	0.932	0.062%
	$\Delta_{u_ana}/\Delta_{u_exp}$	0.25	0.25	0.25	0.27	0.22	0.25	0.248	0.026%
	$\mu_{\Delta_ana}/\mu_{\Delta_exp}$	0.25	0.24	0.27	0.27	0.26	0.29	0.263	0.031%
Confined Kent and Park (1971)	P_{u_ana}/P_{u_exp}	0.96	1.02	0.97	0.97	0.99	1.01	0.987	0.059%
	$\Delta_{u_ana}/\Delta_{u_exp}$	1.00	0.87	0.93	0.90	0.85	0.94	0.915	0.291%
	$\mu_{\Delta_ana}/\mu_{\Delta_exp}$	0.98	0.83	0.98	0.88	1.02	1.10	0.965	0.943%
Modified Kent and Park (1982)	P_{u_ana}/P_{u_exp}	0.99	1.05	0.99	0.99	1.00	1.02	1.007	0.059%
	$\Delta_{u_ana}/\Delta_{u_exp}$	1.08	0.98	0.96	0.97	0.91	0.96	0.977	0.315%
	$\mu_{\Delta_ana}/\mu_{\Delta_exp}$	1.05	0.95	0.99	0.96	1.11	1.10	1.027	0.491%
Muguruma <i>et al.</i> (1980)	P_{u_ana}/P_{u_exp}	0.98	1.03	0.98	0.97	1.00	1.02	0.997	0.059%
	$\Delta_{u_ana}/\Delta_{u_exp}$	0.69	0.51	0.40	0.43	0.54	0.84	0.568	2.806%
	$\mu_{\Delta_ana}/\mu_{\Delta_exp}$	0.66	0.48	0.41	0.42	0.65	0.98	0.600	4.668%
Sheikh and Uzuemi (1982)	P_{u_ana}/P_{u_exp}	0.97	1.03	0.97	0.98	1.00	1.01	0.993	0.059%
	$\Delta_{u_ana}/\Delta_{u_exp}$	1.33	1.47	1.20	1.56	1.05	1.05	1.277	4.583%
	$\mu_{\Delta_ana}/\mu_{\Delta_exp}$	1.22	1.30	1.27	2.01	1.20	1.20	1.367	10.095%
Mander <i>et al.</i> (1988)	P_{u_ana}/P_{u_exp}	0.99	1.06	0.99	0.99	1.01	1.03	1.012	0.082%
	$\Delta_{u_ana}/\Delta_{u_exp}$	1.16	1.12	0.79	0.77	0.87	0.96	0.945	2.747%
	$\mu_{\Delta_ana}/\mu_{\Delta_exp}$	1.11	1.05	0.82	0.75	1.03	1.11	0.978	2.394%
Fujii <i>et al.</i> (1988)	P_{u_ana}/P_{u_exp}	0.97	1.02	0.98	0.97	0.99	1.01	0.990	0.044%
	$\Delta_{u_ana}/\Delta_{u_exp}$	0.92	0.72	0.47	0.49	0.51	0.79	0.650	3.500%
	$\mu_{\Delta_ana}/\mu_{\Delta_exp}$	0.86	0.67	0.47	0.47	0.60	0.90	0.662	3.470%
Saatcioglu and Razvi (1992)	P_{u_ana}/P_{u_exp}	0.98	1.04	1.17	0.99	1.01	1.02	1.035	0.483%
	$\Delta_{u_ana}/\Delta_{u_exp}$	1.11	1.01	0.96	0.97	0.91	0.98	0.990	0.452%
	$\mu_{\Delta_ana}/\mu_{\Delta_exp}$	1.08	0.96	1.00	0.95	1.10	1.17	1.043	0.763%
Hoshikuma <i>et al.</i> (1997)	P_{u_ana}/P_{u_exp}	0.98	1.04	1.16	0.97	0.99	1.01	1.025	0.499%
	$\Delta_{u_ana}/\Delta_{u_exp}$	1.10	1.08	0.77	0.77	0.65	0.89	0.877	3.311%
	$\mu_{\Delta_ana}/\mu_{\Delta_exp}$	1.03	0.99	0.78	0.74	0.76	1.04	0.890	2.072%
Sheikh, Shah and Khoury (1994)	P_{u_ana}/P_{u_exp}	0.90	0.95	1.12	0.91	0.92	0.96	0.960	0.668%
	$\Delta_{u_ana}/\Delta_{u_exp}$	0.28	0.27	0.28	0.29	0.23	0.25	0.267	0.051%
	$\mu_{\Delta_ana}/\mu_{\Delta_exp}$	0.25	0.25	0.28	0.28	0.26	0.29	0.268	0.030%
Modified Fafits and Shah (1997)	P_{u_ana}/P_{u_exp}	0.98	1.04	1.16	0.98	1.00	1.01	1.028	0.466%
	$\Delta_{u_ana}/\Delta_{u_exp}$	1.19	1.07	1.03	0.97	0.91	1.02	1.032	0.906%
	$\mu_{\Delta_ana}/\mu_{\Delta_exp}$	1.11	0.98	1.04	0.93	1.03	1.17	1.043	0.751%
Cusson and Paultre (1994)	P_{u_ana}/P_{u_exp}	0.99	1.06	1.18	1.00	1.02	1.03	1.047	0.487%
	$\Delta_{u_ana}/\Delta_{u_exp}$	1.20	1.12	0.97	0.74	0.74	0.96	0.955	3.599%
	$\mu_{\Delta_ana}/\mu_{\Delta_exp}$	1.11	1.03	0.98	0.71	0.86	1.10	0.965	2.395%
Modified Razvi and Saatcioglu (1999)	P_{u_ana}/P_{u_exp}	0.98	1.04	1.13	0.99	1.00	1.02	1.027	0.303%
	$\Delta_{u_ana}/\Delta_{u_exp}$	1.13	0.99	0.89	0.73	0.89	0.99	0.937	1.803%
	$\mu_{\Delta_ana}/\mu_{\Delta_exp}$	1.05	0.92	0.92	0.69	1.02	1.13	0.955	2.331%

Note: The notations are the same as those used in Table 5.

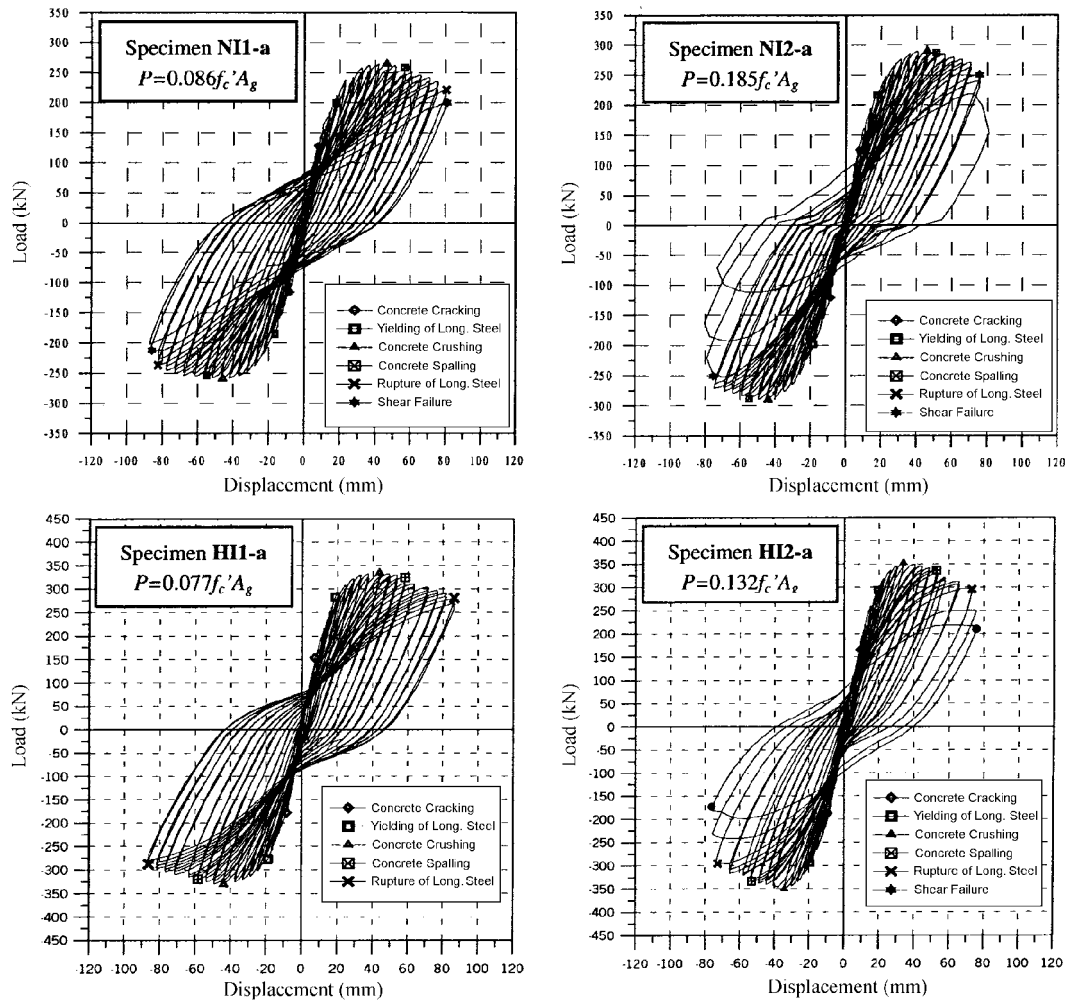


Fig. 5 Hysteretic loops of four specimens

whose predicted results are found to be very close to the experimental results.

6. Conclusions

An analytical model to describe the structural behavior of rectangular reinforced concrete hollow columns is presented. In this model, the thirteen constitutive laws of confined concrete found in literature are used, and the five approaches to estimate the shear capacity are studied. The analytical model has been verified by a series of tests on 12 model columns. It is found that the predicted results are very close to the experimental results. Among the thirteen constitutive models of confined concrete, modified Kent and Park model is found to have the closest results with the tests.

For the specimens with normal strength concrete, the UCSD approach proposed by Priestly *et al.* to estimate the shear capacity gives the best predictions when the test results are compared. For the

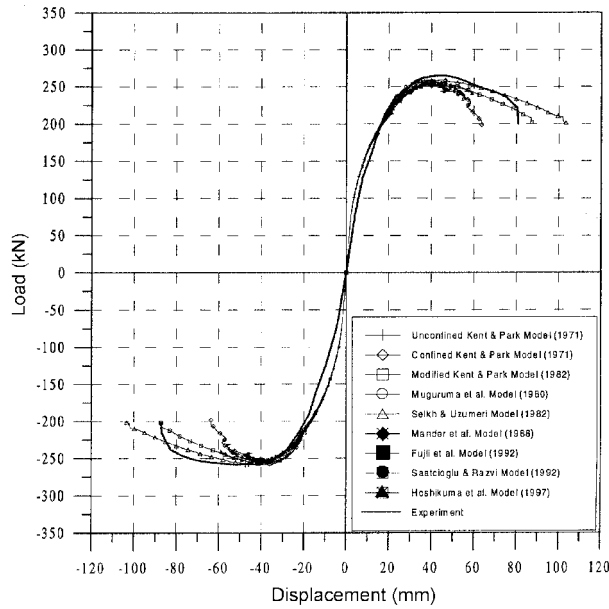


Fig. 6 Lateral loading-displacement of specimen NI1-a, comparison between theoretical predictions and test result

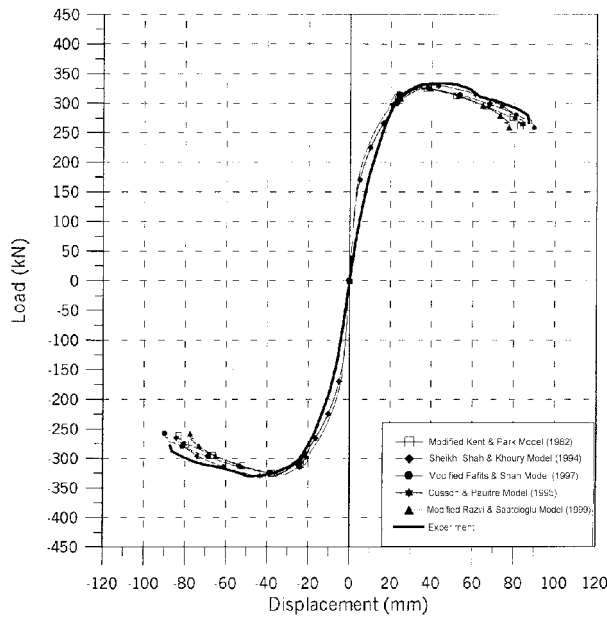


Fig. 7 Lateral loading-displacement of specimen HI1-a, comparison between theoretical predictions and test result

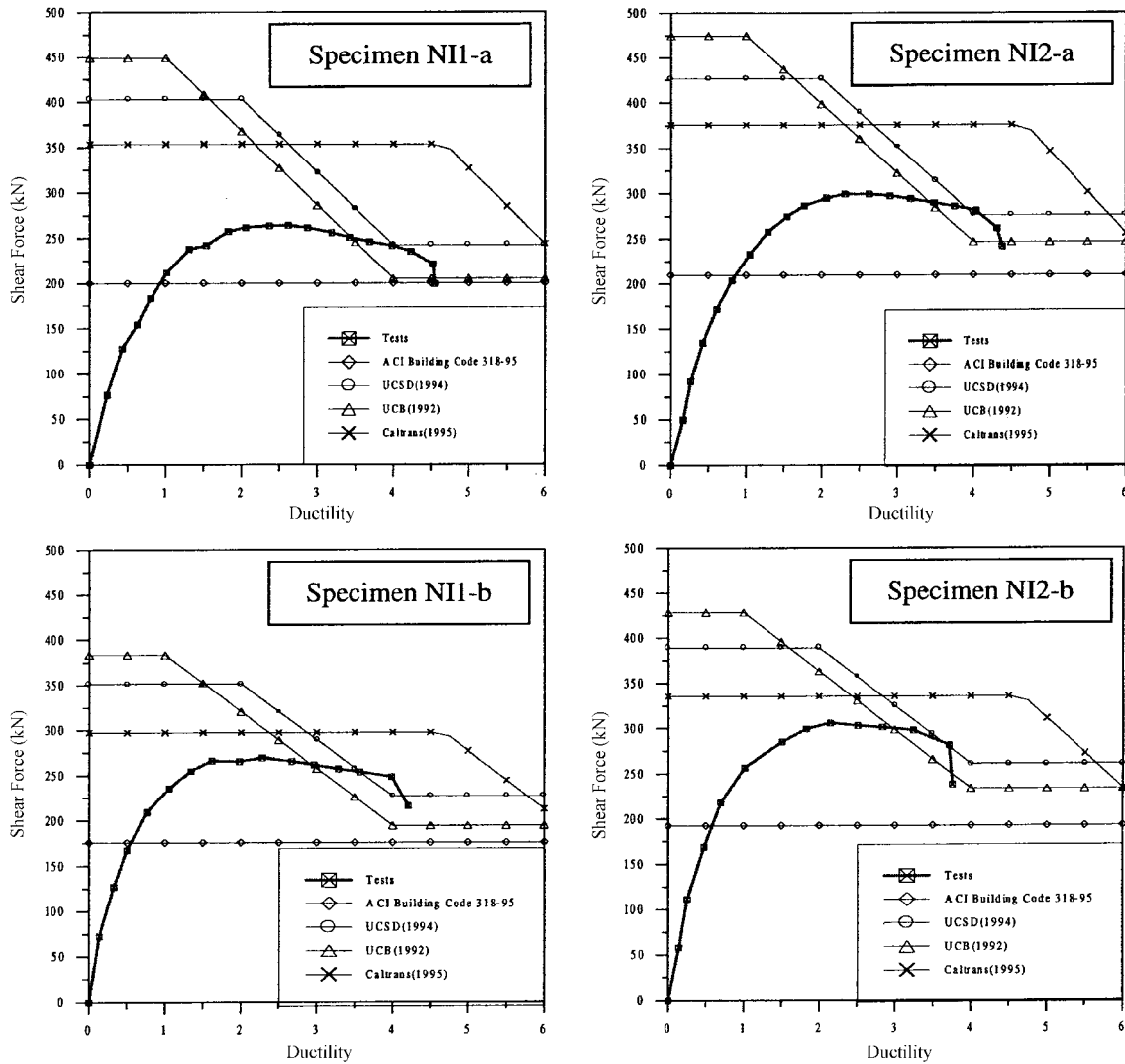


Fig. 8 Theoretical shear capacities compared with tests, normal strength concrete specimens

specimens with high strength concrete, the USC approach proposed by Xiao *et al.* to estimate the shear capacity gives the best predictions when the test results are compared. The other four approaches would possibly overestimate the shear capacity.

Acknowledgements

The research in this paper was funded by the National Science Council, Taiwan through grants NSC 88-2625-Z-006-009 and NSC 87-2621-P-006-011. The authors wish to thank C.Y. Yang, I.C. Nien and S.J. Wang for their assistance in constructing and testing the specimens.

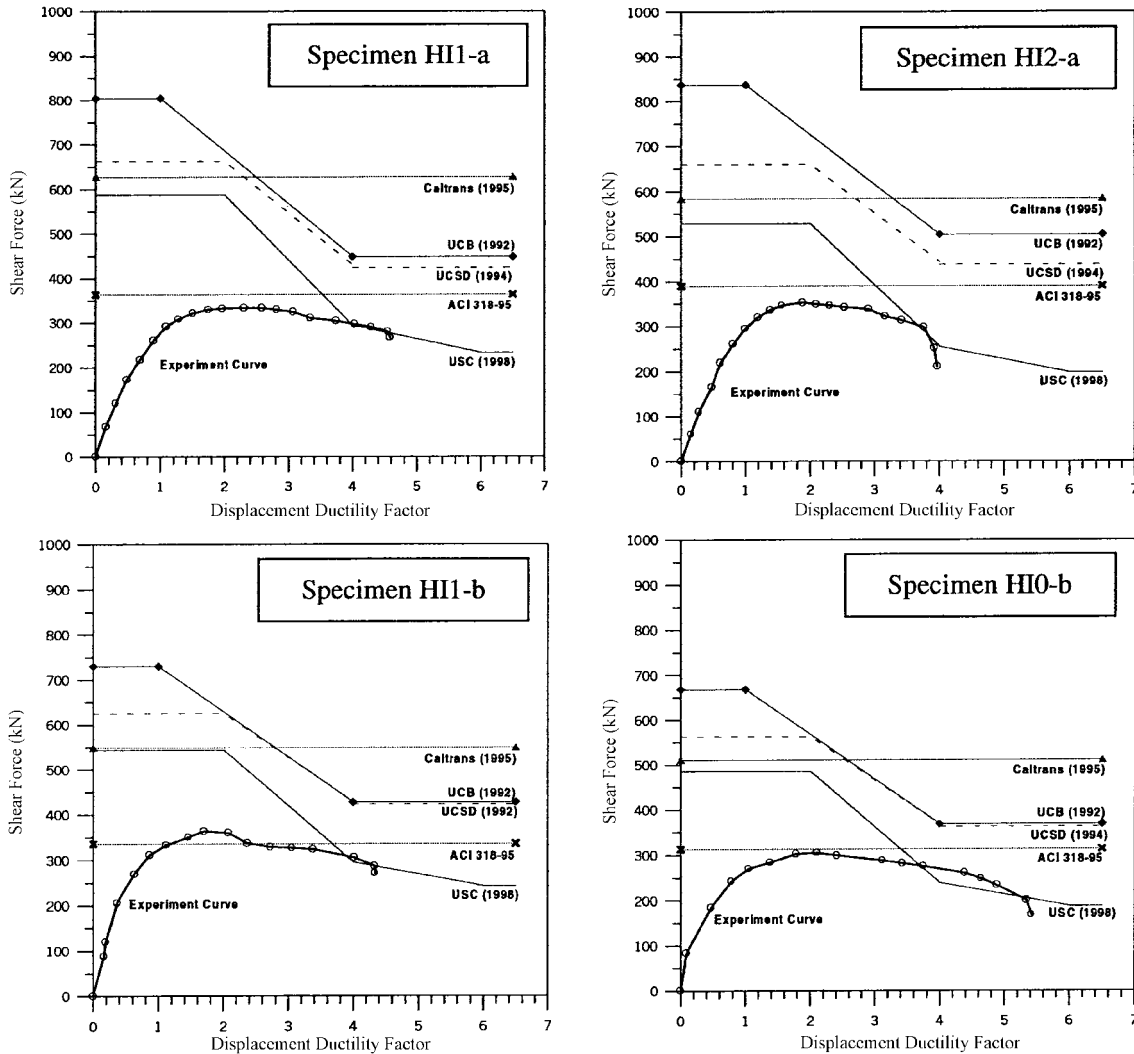


Fig. 9 Theoretical shear capacities compared with tests, high strength concrete specimens

References

- ACI Committee 318 (1995), *Building Code Requirements for Reinforced Concrete (ACI 318-95)*, American Concrete Institute, Detroit, 369.
- Aschhiem, M., Moehle, J.P., and Werner, S.D. (1992), "Deformability of concrete columns", Project Report under Contract No.59Q122, California Department of Transportation, Division of Structure, Sacramento, CA, June.
- Caltrans (1995), "Memo to designers change letter 02", California Department of Transportation, Sacramento, CA., Mar.
- Fujii, M., Kobayashi, K., Miyagawa, T., Inoue, S., and Matsumoto, T. (1988), "A study on the application of a stress-strain relation of confined concrete", *Proc. JCA Cement and Concrete*, Japan Cement Assn., Tokyo, Japan, **42**, 311-314.

- Hong, S.Y. (1998), "Stress-strain relation of confined concrete for rectangular hollow columns (in Chinese)", M.S. theses (supervised by Y.L. Mo), Dept. of Civil Eng., National Cheng Kung University, Taiwan.
- Hoshikuma, J., Kawashima, K., Nagaya, K., and Taylor, A.W. (1997), "Stress-strain for reinforced concrete in bridge piers", *J. Struct. Eng.*, ASCE, May, 624-633.
- Kent, D.C., and Park, R. (1971), "Flexural members with confined concrete", *J. Struct. Div.*, ASCE, **97**(7), 1969-1990.
- Mander, J.B. (1983), "Seismic design of bridge piers", Ph.D. thesis, Department of Civil Engineering, University of Canterbury, Christchurch, New Zealand, Chapter 8.
- Mander, J.B., Priestley, M.J.N., and Park, R. (1988), "Theoretical stress-strain model for confined concrete", *J. Struct. Div.*, ASCE, **114**(8), 1804-1826.
- Mander, J.B., Priestley, M.J.N., and Park, R. (1988), "Observed stress-strain behavior of confined concrete", *J. Struct. Div.*, ASCE, **97**(7), 1969-1990.
- Mander, J.B., Panthaki, F.D., and Kasalanati, A. (1994), "Low-cycle fatigue behavior of reinforcing steel". *J. Mat. In Civ. Eng.*, ASCE, **6**(4), 453-468.
- Matsuda, T. Yukawa, Y., Yasumatsu, Y., Tsukiyama, Y., Ishihara, S., Suda, K., Shimbo, H., and Saito, H. (1996), "Seismic model tests of reinforced concrete hollow piers", *Bridge and Foundation*, Nov., 25-30.
- Mo, Y.L. (1994), *Dynamic Behavior of Concrete Structures*, Elsevier Science B.V., 37-38
- Mo, Y.L. (1998), "Seismic behavior of hollow reinforced concrete columns, (in Chinese)", Research Report, Sinotech Engineering Consultants, April.
- Mo, Y.L., and Jeng, Chyuan-Hwan (1999), "Seismic shear behavior of hollow bridge columns", *Proceedings of The First Int. Conf. on Advances in Struct. Eng. and Mech.*, Seoul, Korea, August.
- Monti, G., and Nuti, C. (1992), "Nonlinear cyclic behavior of reinforcing bars including buckling". *J. Struct. Eng.*, ASCE, **118**(12), 3268-3284.
- Muguruma, H., Watanabe, S., Tanaka, S., Sakurai, K., and Nakaruma, E. (1978), "A study on the improvement of bending ultimate strain of concrete", *PJ. Struct. Eng.*, Tokyo, Japan, **24**, 109-116.
- Muguruma, H., Watanabe, S., and Tanaka, S. (1980), "A stress-strain model of confined concrete", *Proc. JCA Cement and Concrete*, Japan Cement Assn., Tokyo, Japan, **34**, 429-432.
- Park, R., and Paulay, T. (1975), *Reinforced Concrete Structures*, John Wiley & Sons, Inc., 40-45.
- Park, R., Priestley, M.J.N., and Gill, W.D. (1982), "Ductility of square-confined concrete columns", *J. Struct. Div.*, ASCE, **108**(4), 929-950.
- Priestley, M.J.N., Verma, R., and Xiao, Y. (1993), "Shear strength of reinforcement concrete bridge columns", *Second Annual Seismic Research Workshop*, Caltrans, Division of Structures, Mar., 16-18.
- Priestley, M.J.N., Verma, R., and Xiao, Y. (1994), "Seismic shear strength of reinforcement concrete columns", *J. Struct. Engrg.*, ASCE, **120**(7), 2310-2329.
- Priestley, M.J.N., Seible, F., and Calvi, G.M. (1996), *Seismic Design and Retrofit of Bridges*, John Wiley & Sons, Inc., pp.147, 686.
- Razvi, S.R., and Saatcioglu, M. (1999), "Confinement model for high-strength concrete", *J. Struct. Eng.*, ASCE, **125**(3), 281-289.
- Rodriguez, Mario E., Botero, Juan C., and Villa, Jaime (1999), "Cyclic stress-strain behavior of reinforcing steel including effect of buckling", *J. Struct. Engrg.*, ASCE, **125**(6), 605-612.
- Saatcioglu, M., and Razvi, S.R. (1992), "Strength and ductility of confined concrete", *J. Struct. Div.*, ASCE, **118**(6), 1590-1607.
- Sheikh, S.A., and Uzumeri, S.M. (1980), "Strength and ductility of tied concrete columns", *J. Struct. Div.*, ASCE, **106**(5), 1079-1102.
- Sheikh, S.A., and Uzumeri, S.M. (1982), "Analytical model for concrete confinement in tied columns", *J. Struct. Div.*, ASCE, **108**(12), 2703-2722.
- Sheikh, S.A., Shah, D.V., and Houry, S.S. (1994), "Confinement of high-strength concrete columns", *ACI Struct. J.*, **123**(10), 100-111.
- Taylor, A.W., and Breen, J.E. (1994), "Design recommendations for thin-walled box piers and pylons", *Concrete International*, Dec., 36-41.
- Wang, S.J. (1999), "Seismic behavior of precast rectangular hollow columns (in Chinese)", M.S. theses (supervised by Y.L. Mo), Dept. of Civil Engrng., National Cheng Kung University, Taiwan.

Xiao, Y., and Armen Martirosyan (1998), "Seismic performance of high-strength concrete columns", *J. Struct. Eng.*, ASCE, **124**(3), 241-251.

Yao, S.H. (1998), "Flexural behavior of rectangular hollow columns (in Chinese)", M.S. theses (supervised by Y.L. Mo), Dept. of Civil Eng., National Cheng Kung University, Taiwan.

Appendix I: Derivations of load-displacement relationship

1. Ascending branch

(1) Cracking state

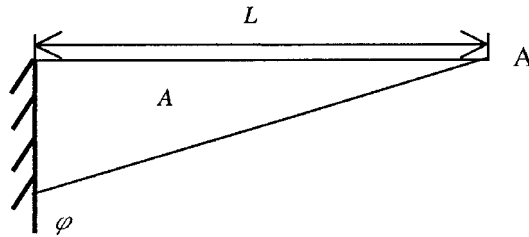


Fig. A1 Illustration of curvature diagram (cracking state)

$$\theta_{cr} = \frac{M_{cr}L}{2EI} \quad (1)$$

$$\delta_{cr} = \theta_{cr} \times L - \frac{1}{3} \times L \times \theta_{cr} = \frac{M_{cr}L^2}{3EI} \quad (2)$$

where

θ_{cr} : rotation angle at cracking

δ_{cr} : lateral displacement at cracking

(2) Yielding state

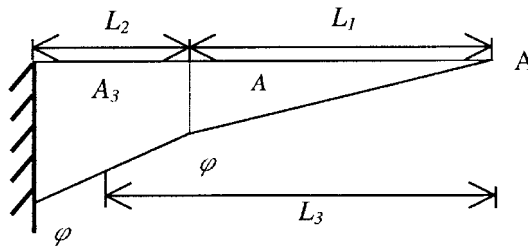


Fig. A2 Illustration of curvature diagram (yielding state)

$$\theta_y = \frac{1}{2} \times L_1 \times \varphi_{cr} + \frac{1}{2} (\varphi_{cr} + \varphi_y) \times L_2 \quad (3)$$

$$\begin{aligned} \delta_y &= \frac{2}{3} \times L_1 \times \frac{1}{2} \times L_1 \times \varphi_{cr} + L_3 \times \frac{1}{2} \times (\varphi_{cr} + \varphi_y) L_2 \\ &= \frac{1}{3} \times \varphi_{cr} \times L_1^2 + \frac{1}{2} \times (\varphi_{cr} + \varphi_y) \times L_2 \times L_3 \end{aligned} \quad (4)$$

where

- θ_y : rotation angle at yielding
- δ_{cr} : lateral displacement at yielding
- L_3 : distance from centroid of area A_3 to end A

(3) Ultimate state

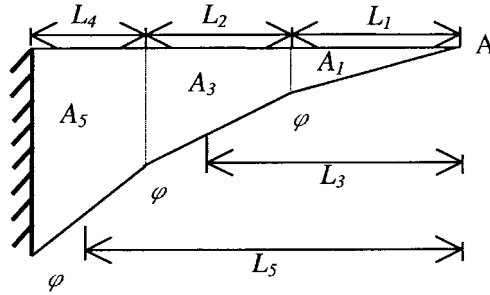


Fig. A3 Illustration of curvature diagram (ultimate state)

$$\theta_u = \frac{1}{2} \times L_1 \times \varphi_{cr} + \frac{1}{2} \times (\varphi_{cr} + \varphi_y) \times L_2 + \frac{1}{2} \times (\varphi_y + \varphi_u) \times L_4 \quad (5)$$

$$\begin{aligned} \delta_u &= \frac{2}{3} \times L_1 \times \frac{1}{2} \times L_1 \times \varphi_{cr} + L_3 \times \frac{1}{2} \times (\varphi_{cr} + \varphi_y) \times L_2 + L_5 \times \frac{1}{2} \times (\varphi_y + \varphi_u) \times L_4 \\ &= \frac{1}{3} \times \varphi_{cr} \times L_1^2 + \frac{1}{2} \times (\varphi_{cr} + \varphi_y) \times L_2 \times L_3 + \frac{1}{2} \times (\varphi_y + \varphi_u) \times L_4 \times L_5 \end{aligned} \quad (6)$$

where

- θ_u : rotation at ultimate state
- δ_u : lateral displacement at ultimate state
- L_3 : distance from centroid of area A_3 to end A
- L_5 : distance from centroid of area A_5 to end A

2. Descending branch

As illustrated in Fig. A4, the curvature in the descending branch can be expressed as

$$\varphi = \varphi_m - \varphi_e + \varphi_r \quad (7)$$

where

- φ : curvature in the descending branch
- φ_m : curvature corresponding to the maximum moment M_m .
- φ_e : elastic restoration curvature.
- φ_r : reloading curvature.

Fig. A5(a) indicates the elastic restoration curvature diagram of a column. The yielding curvature φ_y and the yielding moment M_y correspond to the first yielding of longitudinal bars. The elastic flexural rigidity $(EI)_e$ is the secant modulus at M_y . φ_{cr} and M_{cr} are the curvature and moment at the cracked state, respectively. At the maximum moment state, the column length L can be divided to three regions L_1 , L_2 and plastic hinge length L_p .

It is assumed that the reloading curvature diagram of a column is indicated in Fig. A5(b). Note that the reloading curvature distribution in the plastic hinge region is assumed to be a third order polynomial, which can be determined by using the four boundary conditions (i.e., at the yielding point, the curvature = $\varphi_y M/M_m$

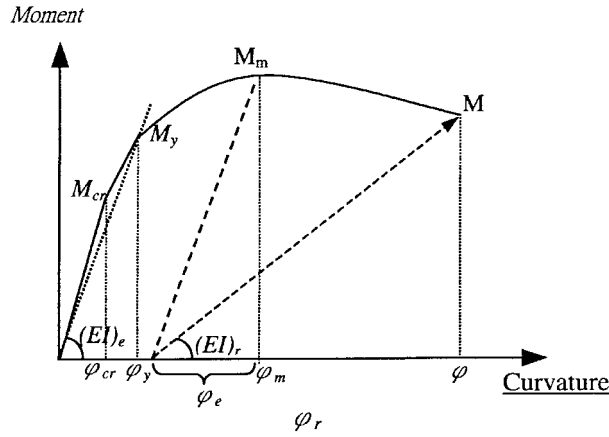
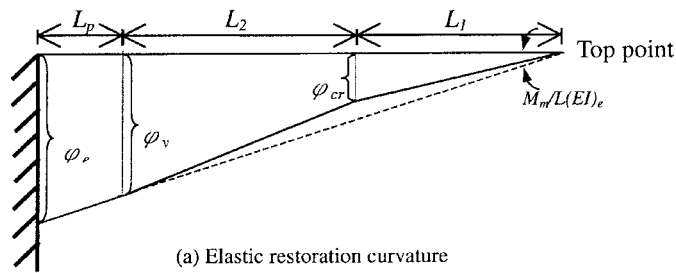
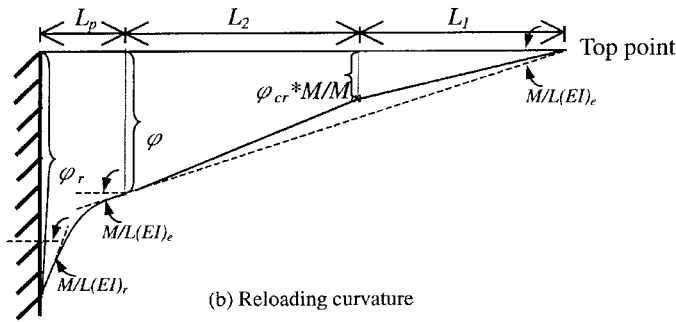


Fig. A4 Moment-curvature curve for descending branch



(a) Elastic restoration curvature



(b) Reloading curvature

Fig. A5 Curvature diagram for descending branch

and the slope of the curvature = $M/L(EI)_e$; at the end point, the curvature = ϕ_r and the slope of the curvature = $M/L(EI)_r$. $(EI)_r$ is the flexural reloading rigidity as shown in Fig. A4.

With the analytical model, the moment-curvature diagram of the bottom section of a column can be obtained. From this moment-curvature diagram, the distribution of curvature in a column can be obtained with the various loads at the top of a column. The corresponding displacement at the top of a column was calculated according to the curvature diagram of the entire column. Then the load-displacement relationship of this column can be established.